Applied Physics Letters

Minority carrier lifetime and photoluminescence of mid-wave infrared InAsSbBi

Cite as: Appl. Phys. Lett. **117**, 061103 (2020); https://doi.org/10.1063/5.0007275
Submitted: 10 March 2020 . Accepted: 24 July 2020 . Published Online: 11 August 2020

Priyanka Petluru, Perry C. Grant, Aaron J. Muhowski, Isabella M. Obermeier, Marko S. Milosavljevic, Shane R. Johnson, Daniel Wasserman, Elizabeth H. Steenbergen, and Preston T. Webster

Applied Physics Letters ARTICLE scitation.org/journal/apl

Minority carrier lifetime and photoluminescence of mid-wave infrared InAsSbBi

Cite as: Appl. Phys. Lett. **117**, 061103 (2020); doi: 10.1063/5.0007275
Submitted: 10 March 2020 · Accepted: 24 July 2020 ·
Published Online: 11 August 2020

Priyanka Petluru,[1] Perry C. Grant,[2,3] Aaron J. Muhowski,[1] Isabella M. Obermeier,[2,4] Marko S. Milosavljevic,[2,3,5] Shane R. Johnson,[5] Daniel Wasserman,[1] Elizabeth H. Steenbergen,[2] and Preston T. Webster[2,a)]

AFFILIATIONS

[1]Department of Electrical and Computer Engineering, University of Texas at Austin, Austin, Texas 78758, USA
[2]Air Force Research Laboratory, Space Vehicles Directorate, Kirtland AFB, New Mexico 87117, USA
[3]Applied Technology Associates, Albuquerque, New Mexico 87123, USA
[4]Department of Electrical and Computer Engineering, University of New Mexico, Albuquerque, New Mexico 87106, USA
[5]Center for Photonics Innovation and Electrical, Computer, and Energy Engineering, Arizona State University, Tempe, Arizona 85287, USA

[a)]**Author to whom correspondence should be addressed:** preston.webster.2@us.af.mil

ABSTRACT

Time-resolved photoluminescence measurements are reported for InAsSbBi alloys grown by molecular beam epitaxy with Bi mole fractions ranging from 0 to 0.8%, yielding minority carrier lifetimes on the order of hundreds of nanoseconds. The minority carrier lifetimes extracted from the time-resolved photoluminescence measurements are comparable to those of lattice-matched InAsSb grown at the same respective temperatures. Nomarski imaging shows that smooth, droplet-free surface morphologies are obtained in 1 μm thick InAsSbBi epilayers grown at temperatures between 360 and 380 °C. The alloy composition-dependent bandgap energies for the InAsSbBi samples are determined from temperature-dependent steady-state photoluminescence measurements and compared with the tetragonal distortion measured by x-ray diffraction to determine the Sb and Bi mole fractions of each sample. The minority carrier lifetime and the achievable extension of the InAsSb(Bi) cut-off wavelength are analyzed as functions of alloy composition and compared with the performance of InAsSb layers with similar growth parameters.

Photodetectors operating in the mid-infrared (mid-IR, 3–5 μm) are of significant interest for a variety of technologically important applications ranging from thermal imaging and sensing to infrared spectroscopy and potentially even free space optical communication. Traditionally, detectors in this wavelength range have been dominated by the HgCdTe material system, although there has been growing interest in the use of strained layer superlattices (SLSs) for mid-IR detection due to their predicted superior performance[1] and the inherent strain/bandgap engineering flexibility afforded by the SLS heterostructure. While InAsSb-based SLS materials have been demonstrated with long minority carrier lifetimes of up to 10 μs,[2] a major technological milestone, the absorption coefficient of the superlattice structures is fundamentally proportional to the square of the electron–hole wavefunction overlap, which, like the effective bandgap of the superlattice, decreases with the increasing period thickness.[3] Consequently, extension of the absorption cutoff to longer wavelengths generally leads to reduced absorption in the superlattice. On the other hand, quaternary InAsSbBi offers the same high level of design flexibility without this decrease in absorption as Bi, being the heaviest group-V element, enables the same mid- to long-wave infrared tunability while maintaining the strong absorption properties of bulk material.[4,5] Since both Bi and Hg share the same core electronic structure, incorporation of Bi into InAsSbBi strongly parallels the effect of Hg in HgCdTe materials. Both constituents act to reduce the bandgap energy and both material systems can be lattice-matched to commercially available substrates, making InAsSbBi, in some ways, an III-V analog of HgCdTe.[4–7]

Although the optical properties, electronic band structure, and alloy composition of ternary and quaternary bismide alloys, including both InAsBi and InAsSbBi, have previously been analyzed through temperature- and excitation-dependent photoluminescence studies, Rutherford backscattering spectrometry, and spectroscopic ellipsometry, among other techniques,[8–12] the minority carrier lifetime of this material system has not been examined. This deficiency in the literature is a result of the trade-offs between efficient bismuth

incorporation and material optical quality. At typical antimonide growth temperatures (close to 400 °C) where optimal optoelectronic properties are obtained in InAsSb-based materials, bismuth incorporation is extremely inefficient, limiting the achievable bandgap reduction. On the other hand, at lower growth temperatures (around 300 °C) where bismuth does incorporate efficiently, the low growth temperature results in a significant degradation of the (now quaternary) material's optical quality,[13] making time-resolved studies challenging. The minority carrier lifetime characterizes the recombination rate in a material and, consequently, is an important metric of optoelectronic quality in materials. As the diffusion length is proportional to the square root of the lifetime, longer minority carrier lifetimes indicate longer minority carrier diffusion lengths, which, in turn, result in higher carrier collection efficiencies. Therefore, the minority carrier lifetime serves as an excellent measure of the potential for InAsSbBi as an absorber material for infrared detectors. In this work, we investigate the minority carrier lifetime of epitaxial InAsSbBi materials as a function of Bi mole fraction and compare the extracted lifetimes with those of bulk InAsSb samples for a range of growth temperatures.

Four InAsSbBi samples are grown on (100)-oriented *n*-type GaSb substrates using a VG-V80H molecular beam epitaxy (MBE) system with valved group-V sources. The InAsSbBi samples consist of a 1 μm thick active region of InAsSbBi, sandwiched between 100 nm and 400 nm layers of lattice-matched InAsSb, which provide a small degree of carrier confinement for photoexcited electron hole pairs. The sample cross section is shown in the inset of Fig. 1. The samples are grown at an In-limited growth rate of 1.0 μm/hour at 360 or 380 °C for the InAsSbBi layer. These conditions produce Bi mole fractions ranging from 0.002 to 0.008 and Sb mole fractions ranging from 0.077 to 0.09 in InAsSbBi, yielding nearly lattice-matched materials. The InAsSb buffer and cap, however, are grown at 440 °C to preserve the quality of the InAsSb buffer on which each InAsSbBi layer is grown and to ensure that the 100 nm cap is of high quality with no

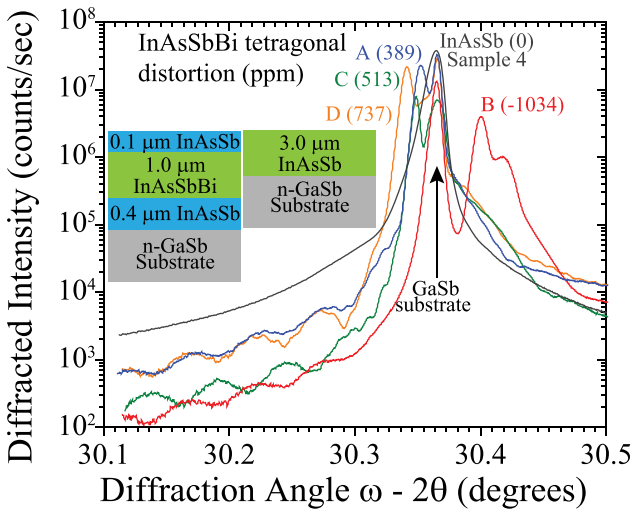

FIG. 1. X-ray diffraction from bulk InAsSb and InAsSbBi samples on GaSb. Parentheses give the tetragonal distortion inferred from the substrate-layer peak separation, in units of parts per million. The inset shows InAsSbBi and InAsSb sample cross sections.

unintentional Bi content in order to provide effective confinement of photogenerated carriers from the surface.

A set of four InAsSb samples, lattice-matched to GaSb substrates, are grown at temperatures between 350 and 440 °C for comparison to the InAsSbBi samples. The InAsSb samples consist of a 3 μm thick layer of InAsSb on a GaSb substrate, intentionally grown thicker than the 1 μm thick InAsSbBi samples to partially compensate for the lack of carrier confinement and to enable more careful examination of surface morphology at lower growth temperatures. The sample cross section is also included in the inset of Fig. 1. Nomarski microscopy is used to evaluate the surface morphology of all the samples under 20× magnification, and the surfaces are determined to be smooth and droplet-free.

The (004) lattice plane x-ray diffraction patterns of the four InAsSbBi samples (samples A–D) and one lattice-matched InAsSb sample grown at an optimal temperature of 440 °C (sample 4) are shown in Fig. 1 and are used to determine the tetragonal distortion in InAsSbBi. The peak from the GaSb substrate is indicated along with the peaks from the InAsSbBi layer in various samples, all of which exhibit strong Pendellösung fringes indicative of high-quality smooth layer interfaces. When the layer strain is small, the tetragonal distortion is described to the first order by the following equation:[5,14]

$$\varepsilon_{\perp} = -\frac{\theta_{InAsSbBi} - \theta_{GaSb}}{\tan(\theta_{GaSb})}. \quad (1)$$

The tetragonal distortion of the InAsSbBi layer in each sample is given in units of ppm in parentheses in Fig. 1 and in Table I. By comparing this lattice distortion with the bandgap energy extracted from photoluminescence measurements, the Bi and Sb mole fractions are obtained.[13] Reciprocal space maps confirm that all the lattice-matched and slightly compressive samples are pseudomorphic, whereas one tensile sample (sample B) is partially relaxed. As a result, the strain and composition analysis of sample B is only approximate.

Photoluminescence is measured from the InAsSb(Bi) samples using a Bruker 80 V Fourier transform infrared spectrometer and a 785-nm wavelength pump laser. The double modulation technique is utilized to increase the signal to noise ratio,[15] with the laser modulated at a frequency of 50 kHz. The steady-state low temperature (120 K) photoluminescence spectra of the bismide samples are shown in Fig. 2, along with the spectrum of InAsSb sample 4 for comparison. Although the 100 nm thick InAsSb cap parasitically absorbs some of the 785-nm wavelength pump laser radiation in the InAsSbBi samples, the hole mobility for InAsSb is determined to be 1186 $cm^2/V\,s$,[16] while the minority carrier lifetime for InAsSb grown at 440 °C is demonstrated later in this work and found to be approximately 1 μs. Based on these values, the minority hole diffusion length is calculated to be 28 μm at 77 K from the following equation:

$$L_h = \sqrt{\mu_h \tau_h kT/e}, \quad (2)$$

where μ_h is the hole mobility, τ_h is the minority carrier lifetime, k is the Boltzmann constant, T is the temperature, and e is the charge of an electron. As the InAsSb diffusion length is much greater than the 100 nm thickness of the cap, electron–hole pairs generated there that do not immediately recombine at the surface are expected to predominately diffuse into and recombine in the lower-bandgap lower-lifetime InAsSbBi region. To further verify that the measured photoluminescence is from

TABLE I. Growth temperatures, tetragonal distortions, bandgap energies, and Sb and Bi mole fractions of InAsSb and InAsSbBi samples.

Sample	Growth temp (°C)	Tetragonal distortion (ppm)	E_g at 120 K (meV)	Sb mole fraction	Bi mole fraction
InAsSb (1)	350	789	299	0.095	0.000
InAsSb (2)	380	626	299	0.094	0.000
InAsSb (3)	410	0	303	0.090	0.000
InAsSb (4)	440	0	309	0.090	0.000
InAsSbBi (A)	380	389	306	0.090	0.002
InAsSbBi (B)	380	−1034	304	0.077	0.004
InAsSbBi (C)	380	513	298	0.082	0.005
InAsSbBi (D)	360	737	281	0.081	0.008

the InAsSbBi absorber region, in one instance the InAsSb cap of bismide sample C is etched down to approximately 35 nm, for the purpose of significantly reducing any potential photoluminescence from the cap while still offering some isolation from surface recombination. The photoluminescence spectra and bandgap energies for both the etched and unetched samples C are found to be approximately the same, indicating that the photoluminescence is indeed from the bismide layer. The photoluminescence peak of the GaSb substrate is not measurable for the bismide samples, due to minimal pump light reaching the substrate at our low excitation powers.

The bandgap energy of each sample is identified at the maximum of the photoluminescence spectrum's first derivative,[17] which identifies the onset of the continuum states at the band edge. This first derivative evaluation enables accurate determination of the bandgap energy without the influence of the Urbach tail slope, which is a function of the growth conditions. Lower peak intensities and extension of the photoluminescence first derivative maxima and peak positions of the bismide samples to wavelengths longer than those of InAsSb with the same degree of strain provide evidence that this luminescence is emitted by InAsSbBi. The Bi and Sb mole fractions of each of the InAsSbBi and InAsSb samples, along with their respective growth temperatures, tetragonal distortions, and bandgaps at 120 K, are provided in Table I.

Temperature-dependent photoluminescence measurements are taken from 4 to 300 K to analyze the bandgap energy as a function of temperature. The temperature-dependent bandgap is included in Fig. 3 for bulk InAsSb sample 4 ($InAs_{0.91}Sb_{0.09}$) and InAsSbBi samples C ($InAs_{0.913}Sb_{0.082}Bi_{0.005}$) and D ($InAs_{0.911}Sb_{0.081}Bi_{0.008}$). The temperature dependence of the bandgap energy is evaluated using the Einstein single oscillator model[17–19] in the following equation:

$$E_g = E_0 - \frac{S_0 k T_E}{\exp\left(\frac{T_E}{T}\right) - 1}, \tag{3}$$

where E_0 is the bandgap energy at 0 K, S_0 is the electron-phonon coupling strength, k is the Boltzmann constant, and T_E is the Einstein

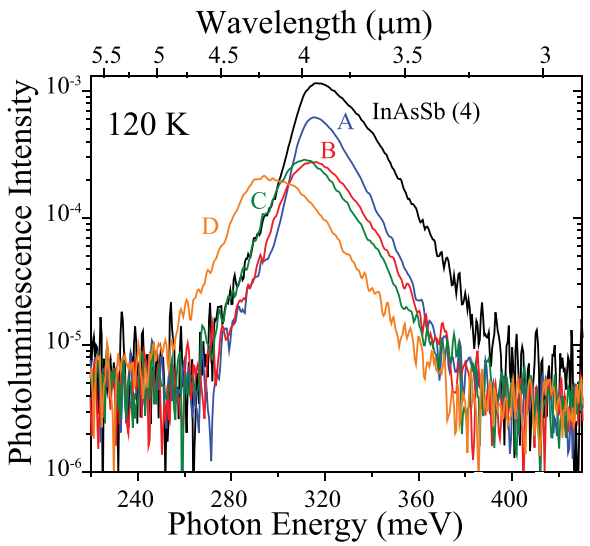

FIG. 2. Photoluminescence from InAsSbBi and InAsSb samples at 120 K, showing the wavelength extension and Urbach slope increase due to the addition of Bi in InAsSb.

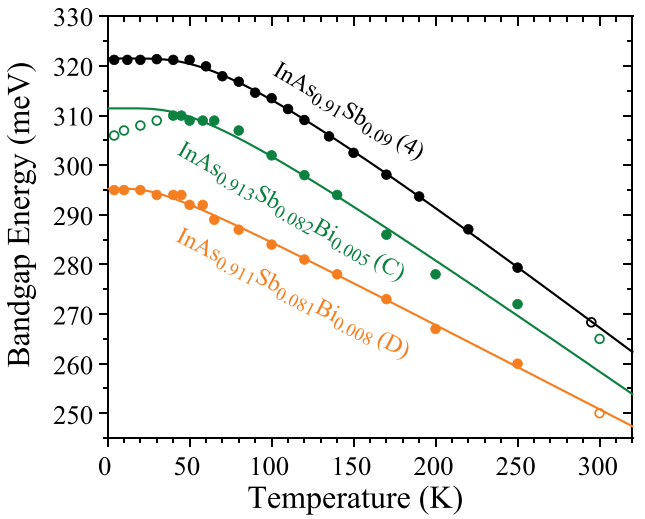

FIG. 3. Bandgap energy of $InAs_{0.91}Sb_{0.09}$, $InAs_{0.913}Sb_{0.082}Bi_{0.005}$, and $InAs_{0.911}Sb_{0.081}Bi_{0.008}$ as a function of temperature (solid circles), with Einstein single oscillator model fits (solid curves). Hollow circles are excluded from the fit and are representative of photoluminescence from localized states (sample C: 4 to 30 K) and noisier photoluminescence at a high temperature (samples 4, C, and D: 295 to 300 K).

temperature. The best-fit parameters for bulk InAsSb sample 4 and bismide samples C and D are included in Table II.

The bandgap energies at 120 K for InAsSb sample 4 and bismide samples C and D are found to be 309 meV (4.01 μm), 298 meV (4.16 μm), and 281 meV (4.41 μm), respectively. The results in Fig. 3 indicate that as the bismuth mole fraction is increased from $InAs_{0.91}Sb_{0.09}$ to $InAs_{0.913}Sb_{0.082}Bi_{0.005}$ to $InAs_{0.911}Sb_{0.081}Bi_{0.008}$, the bandgap energy decreases across all measurement temperatures. The bandgap energy of sample C, or $InAs_{0.913}Sb_{0.082}Bi_{0.005}$, exhibits a blue shift to higher energies between 4 and 40 K, before returning to the traditional bandgap temperature dependence from 40 to 300 K. This may be attributed to radiative recombination from localized band tail states at low temperatures, which has been previously reported in some InAsSbBi and GaAsBi samples.[13,20–23] However, sample D with 0.8% Bi did not exhibit this property, indicating that these states may have some growth condition dependence that can be mitigated.

Time-resolved photoluminescence measurements are also performed on the InAsSbBi and InAsSb samples in order to determine their minority carrier lifetimes. A pulsed 1535-nm laser, with a pulse width of 3.5 ns, is used to excite the samples, while a half waveplate in conjunction with a polarizing beam splitter is used to attenuate the laser to produce low injection conditions in the material. The photoluminescence decays at low pump powers for InAsSbBi samples C and D and InAsSb samples 2 and 4 are shown in Fig. 4(a) at 120 K. The low pump power excitation conditions are 1.6×10^{11} photons/cm^2 per pulse for all the InAsSb samples; 2.2×10^{11} photons/cm^2 per pulse for bismide samples A, B, and C; and 3.1×10^{11} photons/cm^2 per pulse for bismide sample D. These conditions are determined by measuring the laser power per unit area outside the cryostat to obtain the photon flux, which is modified to account for reflection and absorption at the cryostat's CaF_2 window and the sample's cap layer (when present) using optical constants taken from the Handbook of Optical Constants.[24] The handbook does not have optical constants for InAsSb, but they are estimated by shifting the optical constants of InAs by 75 meV to the known bandgap energy of lattice-matched InAsSb. This yields an estimated absorption coefficient of 2.36×10^4 cm^{-1} and a corresponding parasitic loss of about 20% of the 1535 nm wavelength pump excitation in the 100 nm thick InAsSb cap (when present). For the InAsSb samples, when distributed over the 3 μm active region, the result is an excitation of approximately 5.33×10^{14} electron–hole pairs per cm^3, which is comparable with the previously reported background density for this material system, indicating near-low injection conditions.[2,25] When distributed over the 1 μm active region for the bismide samples, the two excitation conditions yield approximately 2.2×10^{15} and 3.1×10^{15} electron–hole pairs per cm^3, respectively, and are also near the cutoff of the low injection regime, which is evident by the pure single exponential decays observed in Fig. 4(a).[26]

TABLE II. Einstein single oscillator model fit parameters for InAsSb sample 4 and InAsSbBi samples C and D.

Sample	E_0 (meV)	S_0	T_E (K)
InAsSb (4)	321.5	2.94	192.1
InAsSbBi (C)	311.5	2.69	154.7
InAsSbBi (D)	295.3	1.99	86.3

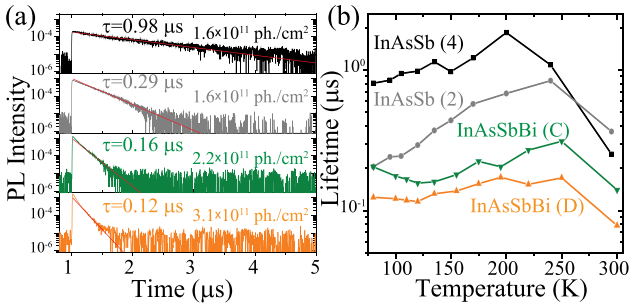

FIG. 4. (a) Time-resolved photoluminescence decays of InAsSb samples 4 and 2 and bismide samples C and D at 120 K. (b) Minority carrier lifetimes of samples 4, 2, C, and D as a function of temperature.

To again ensure that the observed photoluminescence is from the InAsSbBi absorber region rather than the InAsSb cap, time-resolved photoluminescence is also measured using a 3.2-μm laser, which will have almost an order of magnitude larger penetration depth into the samples than the 1535-nm laser. Despite the very different excitation profile, the overall intensity of the photoluminescence decay and the minority carrier lifetimes extracted from the time-resolved photoluminescence performed with the 3.2-μm laser are consistent with those of the 1535-nm pump laser, indicating that the measured photoluminescence is largely from the bismide layer and not the InAsSb cap. If anything, recombination in the InAsSb cap may slightly decrease the measured lifetime, possibly as a result of surface recombination. Thus, the extracted lifetimes for InAsSbBi should be considered a conservative lower bound. Additionally, it is expected that the photon recycling factor should be fairly low (approximately 1.35) given the thicknesses of the cap, absorber, and buffer regions and should therefore not have a significant impact on the minority carrier lifetime.[27]

The time-resolved photoluminescence decay data are fit to a single exponential (solid red line) to determine the minority carrier lifetimes plotted as a function of temperature in Fig. 4(b). The resulting lifetimes for InAsSb sample 4 in Fig. 4(b) demonstrate that the growth chamber is capable of producing high-quality lattice-matched InAsSb with lifetimes exceeding 1 μs. Under higher excitation conditions, a longer decay tail begins to manifest in all of the shorter lifetime bismide samples grown at lower temperatures, which may be the result of increasing luminescence from the more localized states in the Urbach tail of the band edge or from elsewhere in the structure, such as the underlying InAsSb or substrate layers. However, the lifetimes reported are measured under low pump power excitation conditions.

The minority carrier lifetimes of both the InAsSb (squares) and InAsSbBi (circles) samples measured at 120 K are plotted as a function of growth temperature in Fig. 5 for their respective lowest excitation conditions, with error bars reflecting the uncertainty in the chosen fit windows. For these low pump-power conditions, the lifetime data for the InAsSb samples are also fit to a single exponential. The growth parameters (growth temperatures and flux ratios) and the minority carrier lifetimes at 120 K for each sample are presented in Table III.

Figure 5 shows that the minority carrier lifetimes of both the InAsSb and InAsSbBi samples decrease as growth temperature is decreased. The InAsSbBi samples have comparable, though slightly lower, minority carrier lifetimes than the InAsSb samples grown at the

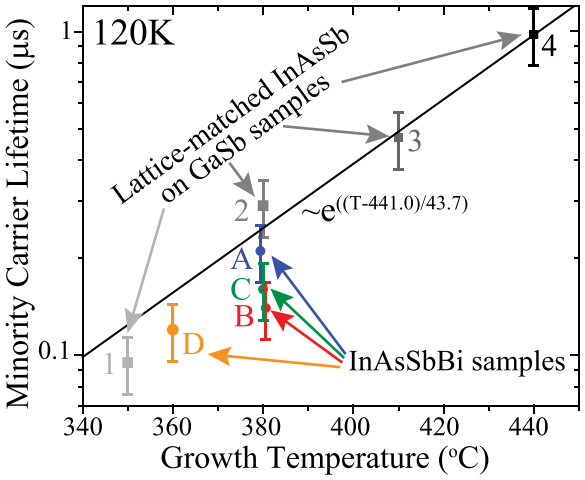

FIG. 5. Minority carrier lifetime of lattice-matched InAsSb (squares) and InAsSbBi (circles) as a function of growth temperature.

same temperatures, which may be due to the slightly leaner As flux conditions utilized to facilitate the incorporation of Bi. Nonetheless, bismide sample A grown at 380 °C has a minority carrier lifetime of 0.21 μs. This value is only slightly lower than the experimentally measured lifetime of 0.29 μs for InAsSb sample 2. Sample D, which is grown at 360 °C, has a minority carrier lifetime of 0.12 μs at 120 K, while an interpolation of the InAsSb lifetime data suggests that an InAsSb sample grown at 360 °C would be expected to have a lifetime of 0.16 μs. Sample B exhibits the lowest minority carrier lifetime at 380 °C, most likely due to the noted partial relaxation in this sample, and overall, the lifetimes for the bismide samples grown at 380 °C appear to increase as the magnitude of the tetragonal distortion decreases. These results indicate that the minority carrier lifetimes of the bismide samples follow the InAsSb trend in Fig. 5 as a function of growth temperature, suggesting that the incorporation of bismuth itself does not negatively impact the minority carrier lifetime. However, the lower growth temperatures (360–380 °C) required to effectively incorporate Bi do seem to adversely affect the optical qualities of the material. Nevertheless, substantial Bi mole fractions on the order of 1% are achieved with smooth surface morphology and technologically relevant minority carrier lifetimes, indicating that future work should endeavor to identify growth conditions that enable this level of Bi incorporation at higher growth temperatures.

TABLE III. Growth temperatures, flux ratios, and minority carrier lifetimes at 120 K of InAsSb and InAsSbBi samples.

Sample	Growth temp (°C)	As/In flux ratio	Sb/In flux ratio	Bi/In flux ratio	Minority carrier lifetime (μs): 120 K
InAsSb (1)	350	1.2	0.1	0	0.095
InAsSb (2)	380	1.2	0.1	0	0.29
InAsSb (3)	410	1.2	0.1	0	0.47
InAsSb (4)	440	1.2	0.1	0	0.98
InAsSbBi (A)	380	1.16	0.085	0.03	0.21
InAsSbBi (B)	380	1.13	0.085	0.06	0.14
InAsSbBi (C)	380	1.16	0.069	0.06	0.16
InAsSbBi (D)	360	1.14	0.081	0.06	0.12

In conclusion, minority carrier lifetimes of bulk InAsSbBi are measured and found to be on the order of hundreds of nanoseconds and generally within 20% of the lifetimes of lattice-matched InAsSb alloys grown at the same temperatures. These results demonstrate that the incorporation of bismuth into InAsSb does not necessarily degrade the minority carrier lifetime, although the growth temperatures of 360–380 °C required for efficient Bi incorporation likely have a deleterious effect on the material's optoelectronic qualities. Additionally, photoluminescence spectra show that the bandgap energy is shifted to longer wavelengths as the bismuth mole fraction is increased, and an absorption cut-off of 4.4 μm in lattice-matched material is demonstrated for a bismuth mole fraction of 0.8% at 120 K; a 0.5 μm wavelength extension beyond traditional lattice-matched InAsSb. Understanding the fundamentals of Bi incorporation and the achievable shift in the alloy band edge provides valuable information for the continuous development of narrow bandgap quaternary alloys for mid-wave infrared applications.

The authors acknowledge financial support through the research sponsored by the Air Force Research Laboratory under Agreement No. FA9453-19-2-0004 and support from the Air Force Research Laboratory Space Vehicles Directorate and University Space Research Association. This work was performed, in part, at the Center for Integrated Nanotechnologies, an Office of Science User Facility operated for the U.S. Department of Energy (DOE), Office of Science by the Los Alamos National Laboratory (Contract No. 89233218CNA000001) and Sandia National Laboratories (Contract No. DE-NA-0003525). In addition, we acknowledge support from an NSF MRSEC (No. DMR-1720595) and the use of facilities within the Eyring Materials Center at Arizona State University supported in part by No. NNCI-ECCS-1542160. Approved for public release: distribution is unlimited. AFMC PA No. 2020-0157; 25 March 2020.

DATA AVAILABILITY

Data are available on request from the authors.

REFERENCES

[1]D. R. Rhiger, "Performance comparison of long-wavelength infrared type II superlattice devices with HgCdTe," J. Electron. Mater. **40**(8), 1815 (2011).
[2]B. V. Olson, E. A. Shaner, J. K. Kim, J. F. Klem, S. D. Hawkins, L. M. Murray, J. P. Prineas, M. E. Flatte, and T. F. Boggess, "Time-resolved optical measurements of minority carrier recombination in a mid-wave infrared InAsSb alloy and InAs/InAsSb superlattice," Appl. Phys. Lett. **101**(9), 092109 (2012).
[3]P. T. Webster, N. A. Riordan, S. Liu, E. H. Steenbergen, R. A. Synowicki, Y.-H. Zhang, and S. R. Johnson, "Absorption properties of type-II InAs/InAsSb superlattices measured by spectroscopic ellipsometry," Appl. Phys. Lett. **106**(6), 061907 (2015).
[4]P. T. Webster, A. J. Shalindar, N. A. Riordan, C. Gogineni, H. Liang, A. R. Sharma, and S. R. Johnson, "Optical properties of InAsBi and optimal designs of lattice-matched and strain-balanced III-V semiconductor superlattices," J. Appl. Phys. **119**(22), 225701 (2016).
[5]P. T. Webster, A. J. Shalindar, S. T. Schaefer, and S. R. Johnson, "Bandgap and composition of bulk InAsSbBi grown by molecular beam epitaxy," Appl. Phys. Lett. **111**(8), 082104 (2017).
[6]A. Rogalski, "HgCdTe infrared detector material: History, status and outlook," Rep. Prog. Phys. **68**, 2267 (2005).

[7]P. Norton, "HgCdTe infrared detectors," Opto-Electron. Rev. **10**(3), 159 (2002).
[8]A. J. Shalindar, P. T. Webster, B. J. Wilkens, T. L. Alford, and S. R. Johnson, "Measurement of InAsBi mole fraction and InBi lattice constant using Rutherford backscattering spectrometry and x-ray diffraction," J. Appl. Phys. **120**(14), 145704 (2016).
[9]Z. M. Fang, K. Y. Ma, R. M. Cohen, and G. B. Stringfellow, "Photoluminescence of InAsBi and InAsSbBi grown by organometallic vapor phase epitaxy," J. Appl. Phys. **68**(3), 1187 (1990).
[10]P. T. Webster, N. A. Riordan, C. Gogineni, S. Liu, J. Lu, X.-H. Zhao, D. J. Smith, Y.-H. Zhang, and S. R. Johnson, "Molecular beam epitaxy using bismuth as a constituent in InAs and a surfactant in InAs/InAsSb superlattices," J. Vac. Sci. Technol., B **32**(2), 02C120 (2014).
[11]R. R. Kosireddy, S. T. Schaefer, A. J. Shalindar, and S. R. Johnson, "Microstructure and surface morphology of InAsSbBi grown by molecular beam epitaxy," J. Appl. Phys. **126**(9), 95108 (2019).
[12]J. Hader, S. C. Badescu, L. C. Bannow, J. V. Moloney, S. R. Johnson, and S. W. Koch, "Auger losses in dilute InAsBi," Appl. Phys. Lett. **112**(19), 192106 (2018).
[13]S. T. Schaefer, R. R. Kosireddy, P. T. Webster, and S. R. Johnson, "Molecular beam epitaxy growth and optical properties of InAsSbBi," J. Appl. Phys. **126**(8), 83101 (2019).
[14]Z. R. Wasilewski, M. M. Dion, D. J. Lockwood, P. Poole, R. W. Streater, and A. J. SpringThorpe, "Composition of AlGaAs," J. Appl. Phys. **81**(4), 1683 (1997).
[15]A. R. Reisinger, R. N. Roberts, S. R. Chinn, and T. H. Myers II, "Photoluminescence of infrared-sensing materials using an FTIR spectrometer," Rev. Sci. Instrum. **60**(1), 82 (1989).
[16]L. K. Casias, *Transport in Mid-Wavelength Infrared (MWIR) p- and n-Type InAsSb and InAs/InAsSb type-II Strained Layer Superlattices (T2SLs) for Infrared Detection* (University of New Mexico, 2019).
[17]P. T. Webster, N. A. Riordan, S. Liu, E. H. Steenbergen, R. A. Synowicki, Y.-H. Zhang, and S. R. Johnson, "Measurement of InAsSb bandgap energy and InAs/InAsSb band edge positions using spectroscopic ellipsometry and photoluminescence spectroscopy," J. Appl. Phys. **118**(24), 245706 (2015).
[18]S. R. Johnson and T. Tiedje, "Temperature dependence of the Urbach edge in GaAs," J. Appl. Phys. **78**(9), 5609 (1995).
[19]L. Viña, S. Logothetidis, and M. Cardona, "Temperature dependence of the dielectric function of germanium," Phys. Rev. B. **30**(4), 1979 (1984).
[20]N. A. Riordan, C. Gogineni, S. R. Johnson, X. Lu, T. Tiedje, D. Ding, Y.-H. Zhang, R. Fritz, K. Kolata, S. Chatterjee, K. Volz, and S. W. Koch, "Temperature and pump power dependent photoluminescence characterization of MBE grown GaAsBi on GaAs," J. Mater. Sci. **23**, 1799 (2012).
[21]T. M. Christian, K. Alberi, D. A. Beaton, B. Fluegel, and A. Mascarenhas, "Spectrally resolved localized states in $GaAs_{1-x}Bi_x$," Jpn. J. Appl. Phys., Part 1. **56**, 035801 (2017).
[22]A. R. Mohmad, F. Bastiman, C. J. Hunter, R. Richards, S. J. Sweeney, J. S. Ng, and J. P. R. David, "Effects of rapid thermal annealing on $GaAs_{1-x}Bi_x$ alloys," Appl. Phys. Lett. **101**(1), 012106 (2012).
[23]G. Pettinari, A. Polimeni, M. Capizzi, J. H. Blokland, P. C. M. Christianen, J. C. Maan, E. C. Young, and T. Tiedje, "Influence of bismuth incorporation on the valence and conduction band edges of $GaAs_{1-x}Bi_x$," Appl. Phys. Lett. **92**(26), 262105 (2008).
[24]E. D. Palik and R. T. Holm, *Handbook of Optical Constants of Solids* (Academic Press, San Diego, 1985).
[25]B. V. Olson, *Time-Resolved Measurements of Charge Carrier Dynamics and Optical Nonlinearities in Narrow-Bandgap Semiconductors* (University of Iowa, 2013).
[26]B. V. Olson, E. A. Kadlec, J. K. Kim, J. F. Klem, S. D. Hawkins, and E. A. Shaner, "Intensity- and temperature-dependent carrier recombination in InAs/In(As,Sb) type-II superlattices," Phys. Rev. Appl. **3**(4), 044010 (2015).
[27]L. Höglund, D. Z. Ting, A. Soibel, A. Fisher, A. Khoshakhlagh, C. J. Hill, S. Keo, and S. D. Gunapala, "Minority carrier lifetime in mid-wavelength infrared InAs/InAsSb superlattices: Photon recycling and the role of radiative and Shockley-Read-Hall recombination mechanisms," Appl. Phys. Lett. **105**(19), 193510 (2014).